Progress In Electromagnetics Research C, Vol. 172, 312–323, 2026

PIER C

(Received 27 May 2026, Accepted 9 July 2026, Scheduled 12 August 2026)

A Dual Broadband Eight-Element MIMO Antenna with R-Shaped Slot Loaded Patch and Grid-shaped Modified Ground Plane for Sub-6 GHz 5G Applications

Sunera G. Kargathara[1,*], Shobhit K. Patel[2], and Sudipta Das[3]

[1]Department of Information and Communication Technology, Marwadi University, Rajkot, Gujarat 360003, India
[2]Department of Computer Engineering, Marwadi University, Rajkot, Gujarat 360003, India
[3]Department of Electronics & Communication Engineering, IMPS College of Engineering and Technology, West Bengal, India

ABSTRACT: A miniature-sized dual-broadband eight-element Multiple-Input Multiple-Output (MIMO) antenna with R-shaped radiators in the sub-6 GHz band for 5G applications is presented in this research article. The proposed novel MIMO configuration includes 4×2 antennas mounted on a $60 \times 112\,\text{mm}^2$ substrate with each radiator measuring $28 \times 28\,\text{mm}^2$. Modified Ground Structure (MGS) is employed to enhance impedance matching and reduce the effect of electromagnetic interaction between closely placed radiators. The MGS and optimal R-shape design enable this MIMO antenna to work at dual frequencies. Two resonances at frequencies of 1.8 GHz (1.67–2.03 GHz) and 4.4 GHz (4.15–4.75 GHz) are observed in both simulations and measurements, and the maximum reflection coefficient is recorded at -28 dB, which implies that excellent impedance matching is achieved for the designed eight-port radiator. This antenna design offers isolation better than 15 dB in both operating frequency bands (1.67–2.03 GHz and 4.15–4.75 GHz), with a maximum isolation of about 40 dB at certain frequencies. Moreover, it is found that the proposed antenna has good diversity parameters with Envelope Correlation Coefficient (ECC) < 0.01 and Diversity Gain (DG) around 10 dB. The results show that this novel antenna is capable of providing a suitable balance among small size, strong isolation, stability of radiation, and enhanced diversity performance, thereby becoming an excellent choice for sub-6 GHz 4G/LTE cellular communications and 5G applications.

1. INTRODUCTION

The rapid advancements in wireless technology, especially in sub-6 GHz frequency bands, have increased the need for smaller sizes and better performance of MIMO antennas. The major problems associated with the incorporation of multiple antenna elements in the same space include mutual coupling, mismatched impedance, and the degradation of radiation properties [1–3]. The inclusion of multiple antennas into miniature wireless communication devices brings some serious problems, such as mutual coupling effects, impedance matching problems, decreased radiation efficiency, and correlation among antenna elements [1, 4, 5]. To address these issues, techniques such as isolation improvement and decoupling methods have been reported in recent times. In particular, modifications in the ground plane can effectively reduce surface-wave currents and minimize electromagnetic coupling between adjacent antennas without increasing size [6–8]. Likewise, there have been extensive studies on the application of electromagnetic bandgap (EBG) structures and neutralization line techniques to enhance the isolation and impedance bandwidth performance. Even though these techniques offer excellent performance improvements, their increased fabrication difficulties, required extra size, and potential parasitic effects are also noteworthy challenges [6, 9, 10]. Alongside traditional decoupling techniques, several other novel antenna design concepts have been proposed to improve the efficiency of miniaturized MIMO antennas. Fractal configurations have been employed to provide multiband behavior and miniaturization, while the employment of parasitic elements and metamaterial-based configurations has been proven to yield better gain, bandwidth, and radiation efficiency [2, 11–13]. Recently, artificially engineered metasurface-based devices have attracted researchers' attention because of their high potential for improving the efficiency of wireless communication systems [14, 15]. In recent times, research efforts concerning eight-element MIMO antennas, most studies have focused on good isolation, low ECC, and diversity properties, which will facilitate fast wireless applications and transmission of large amount of data [1, 9, 12]. Even though considerable progress has been made in the past few years, many of the suggested designs still have shortcomings such as bulky construction, complicated decoupling schemes, and increased structural complexity [9, 16, 17]. Recently, geometry-based antennas have become a highly useful approach in designing compact MIMO structures. With optimal geometry and arrangement of the radiators, the desired impedance profile, reduced mutual coupling, and improved current distribution can be achieved without using any other decoupling mechanism [16, 18, 19]. It is evident from the recent research of sub-6 GHz MIMO antennas that there is increasing interest in antenna systems that operate in the frequency range of 3–5 GHz for next-generation wireless devices. Following these benefits

* Corresponding author: Sunera G. Kargathara (sunera.kargathara@marwadieducation.edu.in).

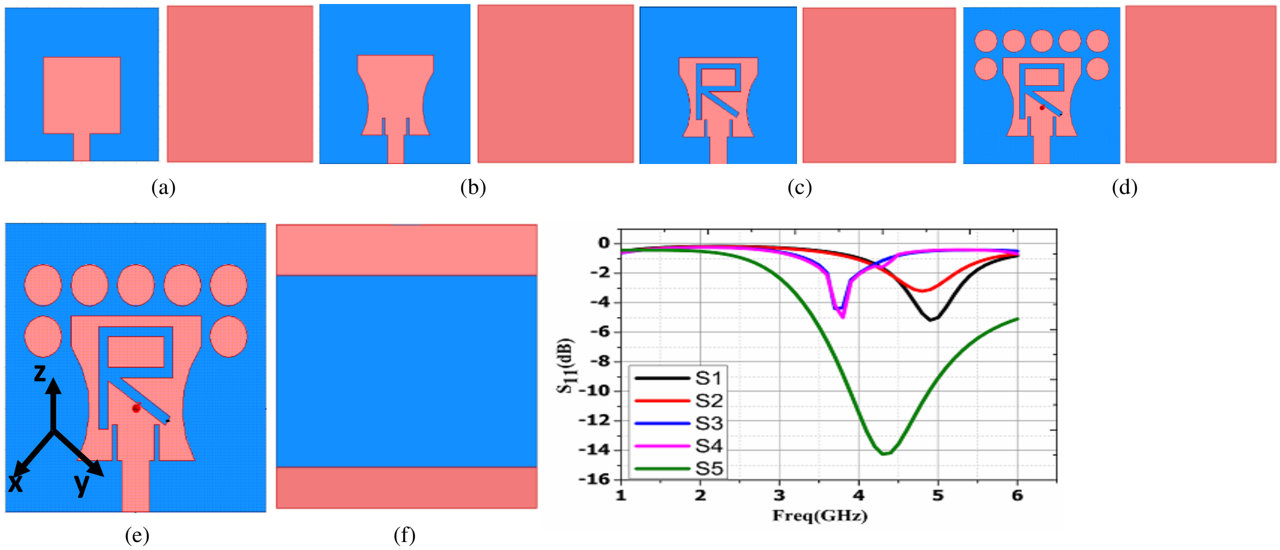

FIGURE 1. Evolution of the proposed R-shaped antenna element and corresponding reflection coefficient characteristics. (a) Conventional rectangular radiator, (b) radiator with modified side profile, (c) radiator incorporating the R-shaped slot, (d) final patch with circular elements, (e) proposed antenna with modified ground structure (MGS), and (f) simulated reflection coefficient (S_{11}) comparison for different stages.

of the geometrically optimized antennas, this work suggests a novel R-type radiating element-based eight-element compact MIMO antenna design with a modified ground plane, featuring circular slots. The objective of this research article is to propose an eight-element, compact MIMO antenna that has been optimized for sub-6 GHz wireless applications. Consequently, the developed antenna design operates in the 1.67–2.03 GHz and 4.15–4.75 GHz frequency bands allowing using the same antenna for LTE/4G and sub-6 GHz applications [19–22]. The proposed antenna design tries to balance among miniaturization, wide isolation, high bandwidth, improved gain characteristics, and reduced design complexity [23–25]. The impact of the suggested R-shape radiator with circular-slot DGS on the antenna performance is analyzed via simulations. The designed antenna shows a beneficial trade-off among size, gain, and complexity for sub-6 GHz MIMO systems. The reason for 1.8 GHz and 4.4 GHz frequency bands is the practical applicability of these bands for wireless communication systems in current conditions and in the future. Specifically, the 1.8 GHz band is related to LTE Band 3 and 5G NR Band n3 that are still widely applied due to good combination of propagation coverage, penetration capacity, and spectral efficiency. At the same time, the frequency band 4.4 GHz is related to the sub-6 GHz mid-band spectrum, which has become one of the most attractive candidates for deployment in 5G due to much higher data throughput compared to conventional cellular bands, providing sufficient coverage at the same time.

The major key findings are summarized as follows:

- The designed geometry comprised novel R-shaped slot-loaded radiating patches surrounded by circular parasitic elements and a grid type modified connected ground plane.
- The design and analysis of single-element, two-element, and four-element MIMO models are also included along with the proposed eight-element antenna.
- The proposed eight-element MIMO antenna exhibits dual broadband performance, operating at 1.8/4.4 GHz with 19.45% and 13.48% fractional bandwidths.
- The proposed design achieves gains that are above 9 dB in the lower band and around 2 dB to 10 dB in the upper band.
- The ECC < 0.01 and DG $\sim$ 10 dB values ensure strong diversity performance.
- It shows stable radiation patterns and excellent impedance matching at resonance bands.
- Performance validation via realizing prototype and its experimental validation in an anechoic chamber.
- The suggested 8-port MIMO model, operating at 1.8 GHz (1.67–2.03 GHz) and 4.4 GHz (4.1–4.75 GHz) is ideal for multiband wireless services. It simultaneously supports 4G/LTE cellular communications, sub-6 GHz 5G, and various specialized C-band or S-band systems, maximizing connectivity from a single unit.

2. EVOLUTION OF THE MIMO CONFIGURATION

This section discusses design evolution stages of the intended single-element antenna along with the proposed geometries and associated results of the single-element antenna, two-port and four-port MIMO antennas in Subsections 2.1, 2.2, and 2.3, respectively, which were analyzed before modeling the eight-element-based MIMO radiator system. Finally, the configuration of the proposed 8-port MIMO model is described in Subsection 2.4.

2.1. Single-Element Antenna Configuration with Analysis of Parametric Study

The development of the proposed antenna is shown in Figures 1(a)–(e), in which the shape is altered to achieve the intended dual-frequency performance. The reflection coef-

TABLE 1. Optimized geometrical parameters of the proposed antenna.

Parameter	Description	Value
L	Overall substrate length	112 mm
W	Overall substrate width	60 mm
S1	FR-4 substrate thickness	1.6 mm
ε_r	Relative permittivity of FR-4	4.4
tan δ	Loss tangent of FR-4	0.02
W1	Width of the line R-shaped radiating element	1 mm
R1	Radius of the circular parasitic element	2 mm
R2	Edge-to-edge spacing between adjacent circular parasitic elements	1 mm
Lf	Length of the microstrip feed line	5 mm
Wf	Width of the microstrip feed line	3 mm
Li	Inset feed depth	3.5 mm
Wi	Inset feed width	0.5 mm
Gs	Width of each strip in the modified ground structure (MGS)	4 mm
Gg	Gap between adjacent strips of the modified ground structure (MGS)	19 mm
d1	Horizontal center-to-center spacing between adjacent antenna elements	14 mm
d2	Vertical center-to-center spacing between adjacent antenna elements	12 mm

ficients for various development stages are included in Figure 1(f). At the initial stage, an ordinary rectangular patch (Stage S1) was used as the radiator. However, the antenna did not match properly to the impedance and resonates at an resonated outside the desired frequency range. To solve the impedance mismatch problem in Stage S2, the rectangular patch was changed to an R-shaped radiator by cutting particular parts from the rectangular patch. By doing this, the overall length of the electric current has been increased while retaining the radiator's small dimensions, thus changing the resonant frequency to the desired higher frequency of 4.4 GHz. To enhance the performance of the upper-band antenna, circular loading elements were used around the radiator in Stage S3. For Stage S4, parasitic elements in a circular pattern have been added to the upper region of the radiator. Parasitic elements influence the electromagnetic field around the radiator and redistribute surface current without increasing the antenna's physical size. Thus, the impedance bandwidth in the region 4.4 GHz is improved. However, the single-element antenna is still limited to the upper frequency band.

The proposed antenna with dimensional parameters, stub radius ($R1 = 2$ mm), and width of line in R shape ($W1 = 1$ mm) is shown in Figure 2(a). Geometrical parameters such as $W1$ and $R1$ play a crucial role in performance optimization. Furthermore, the height of the dielectric substrate also has a powerful impact on antenna resonance. The results of parametric studies are shown in Figures 2(b)–(d). The parameter $R1$ denotes the radius of circular parasitic patches, and $W1$ indicates the width of a specific portion of the etched "R" slot. Figure 2(b) compares three different radii of the circular parasitic patches to investigate their impact on impedance matching and resonance characteristics. $R1 = 1$ mm (black color) shows the shallowest resonance; $R1 = 1.5$ mm (red line) indicates an intermediate resonance depth; and $R1 = 2$ mm (blue color) results in the deepest S_{11} dip of approximately -14 dB. A deeper dip (lower dB value) means less power is reflected, making the antenna more efficient at 4.5 GHz as $R1$ increases. Hence, $R1 = 2$ mm is opted as the proposed dimension for the antenna. In a similar pattern, the effects of $W1$ parameter on the resonance of the designed antenna are analyzed by varying its dimensions, as shown in Figure 2(c). The antenna resonates between 4 and 5 GHz where the S_{11} curves drop below -10 dB. The analysis of $W1$ can be summarized as that $W1 = 1.2$ mm shows the slowest resonance, reaching approximately -12.5 dB. $W1 = 0.8$ mm improves matching, but increasing $W1$ to 1 mm (proposed) provides the best impedance matching and broadest bandwidth. The investigation on various substrate thicknesses ($S1$) has been carried out, and the outcomes are shown in Figure 1(d). With increasing height from 0.8 mm to 1.6 mm, impedance matching becomes much improved since the minimum value of S_{11} decreases from -7.5 dB to -14 dB. This is due to the better fringing effect and improved coupling between the feed and radiating patch of the antenna. A substrate height of 1.6 mm is chosen for the antenna design due to its good impedance matching capability.

The optimized geometric dimensions for the proposed antenna are given in Table 1. The dimensions provided here include those for the radiator, inset-fed microstrip line, modified ground plane, and spacing between radiators, ensuring that the proposed antenna is easily reproduced.

The surface current distribution of the designed R-shaped radiating structure at the resonant frequency is shown in Figures 2(e)–(f). As can be seen from the figure, the highest current density is along the microstrip feed line and the lower vertical part of the R-shaped radiator, meaning that these parts play a key role in excitation of the fundamental resonance mode. The propagation of the current through the radiator continues by following the external contour of the R-shaped slot and circling

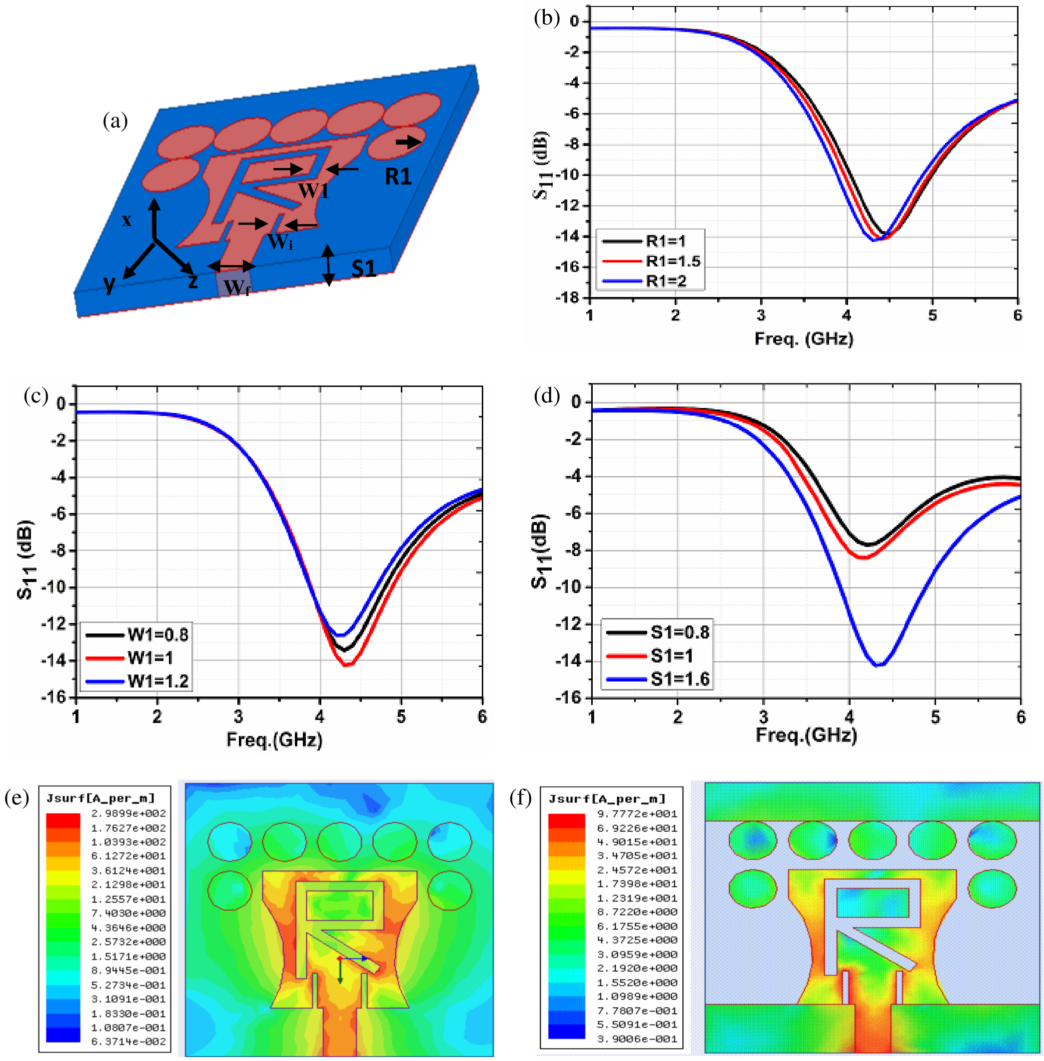

FIGURE 2. Design and analysis of single-element antenna. (a) Suggested geometry of the R-shaped antenna, and parametric study, (b) S_{11} characteristics of the single R-shaped antenna by changing $R1$, (c) S_{11} characteristics by changing $W1$, (d) S_{11} characteristics by changing dielectric substrate thickness ($S1$), (e) surface current at 4.4 GHz with full ground, and (f) surface current at 4.4 GHz with MGS.

along the rectangular loop, extending the current path without increasing the radiator's size. Thus, extending the current path reduces resonant frequency and improves impedance matching. A significant current concentration is also noted along the inclined part of the R-shaped slot, meaning that it is one of the main factors providing the excitation of the higher resonance frequency. In turn, weak currents are excited on the circular parasitic resonators, which means that their main function is a parasitic resonator to provide impedance tuning and bandwidth improvement.

2.2. Two-Element Configuration

Figure 3 illustrates the structure and performance of a two-element R-shaped MIMO antenna. The layout in Figure 3(a) shows a dual-antenna system designed for MIMO applications, which is used to improve data throughput and link reliability in wireless communications. To investigate the behavior of the proposed R-shaped radiator, a two-element configuration was initially developed. Two identical R-shaped elements are placed in close proximity and excited using separate microstrip feed lines. The primary radiating elements are shaped as the letter "R". Non-standard shapes like this are often used to create multiple current paths, which helps achieve multiband resonance. In addition, surrounding the R-shaped patches, several parasitic circular metallic disks are included to improve their performance.

S_{11} characteristic of the two-element R-shaped antenna is shown in Figure 3(b). The antenna exhibits dual-band resonance, with a dominant resonance at approximately 3.7 GHz where the S_{11} reaches approximately -19 dB, indicating good impedance matching in this frequency region. At lower frequencies, the antenna shows relatively less matching, with S_{11} value approximately -13 dB below about 1.5 GHz. With increasing the frequency above the primary resonance point, impedance matching deteriorates, causing S_{11} to approach values between -8 dB and -9.5 dB. The resonance phenomenon is mainly explained by the fact that the current on the radi-

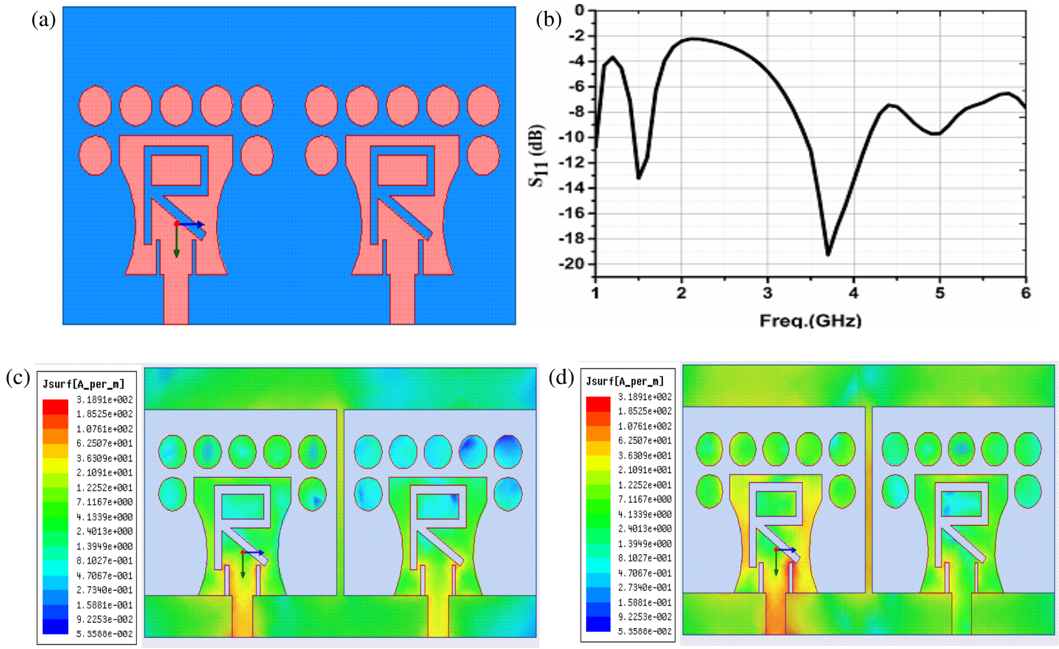

FIGURE 3. Two-element MIMO antenna. (a) Layout, (b) S_{11} response of the two-element R-shaped MIMO antenna, (c) surface current distribution at 1.5 GHz, and (d) surface current distribution at 3.7 GHz.

ator occurs within the R-shaped structure, thereby extending the electrical path. Nevertheless, because of the small number of elements, only two elements were used in the circuit. Therefore, the number of extra resonances is limited, making the bandwidth rather narrow. The deep resonance at 3.7 GHz suggests that it is for applications in that range, which is common for 5G sub-6 GHz or WiMAX applications. Figures 3(c) and (d) show the simulated current distribution on the surface of the proposed MIMO antenna at resonant frequencies of 1.5 GHz and 3.7 GHz when Port 1 is excited, and other ports are terminated with 50 Ω. From the figure, it can be seen that the maximum current density exists on the microstrip feed line and the lower portion of the R-shaped radiator; therefore, it is clear that these are the two main components of antenna excitation. The current flows through the rectangular loop and the inclined part of the R-shaped slot; hence, the effective length increases, and dual-band resonance is obtained. It is also evident that there is no induced current density on the adjacent radiator; hence, it is clear that the proposed grid-type modified ground plane efficiently eliminates surface waves and minimizes electromagnetic coupling between adjacent antenna elements. There is not much current density on the circular parasitic elements; therefore, these elements do not act as active radiators, but they help tune impedance and redistribute the current.

2.3. Geometrical Layout of the Four-Element Antenna

In this subsection, the geometric design of a 4-port (2 × 2) MIMO antenna system, featuring four radiating patches and a modified ground structure (MGS), is presented and discussed. Figure 4(a) shows the top view of the proposed 4-element MIMO antenna. The antenna comprises four identical radiating elements arranged in a 2×2 matrix. Each patch has an R-shaped geometry. The radiators include specific slots to create a multi-band resonance with improved matching. Each patch is fed by an inset-feed microstrip line to ensure proper impedance matching. The symmetrical configuration enables the distribution of uniform currents over the antenna surface, whereas the circular parasitic patches function as decoupling elements that prevent the propagation of surface waves. The bottom layer (right image) shows the modified Ground Structure (MGS), as shown in Figure 4(b). Instead of a solid metal sheet, it contains wide horizontal and narrow vertical slots. The slots introduce additional capacitance or inductance, helping the antenna resonate across frequency bands, such as 5G sub-6 GHz or WLAN. Despite the slots, the ground plane remains largely interconnected to provide a common reference plane and a stable radiation pattern.

The S_{11} of the four-element R-shaped antenna array is illustrated in Figure 4(c). It can be clearly seen that the S_{11} of this structure shows much better results than the 2-port MIMO configuration, especially in the lower operating band. Its lower band response reaches a deeper 14.5 dB. However, it shows more fluctuations/ripples in the 1.0–1.3 GHz range. The response in the upper band is slightly broader with an improved S_{11} of −19.6 dB. The obtained results show that the shift from single-element structure to multi-element design greatly improves the antenna impedance due to introducing several resonant points. The observed phenomena are mainly caused by interaction between elements and, consequently, increase in the length of the current paths, providing opportunities for multiband operation. However, further improvements are required to achieve broadband performance. Surface current distributions of the 4-element MIMO structure proposed at 1.5 GHz and 3.7 GHz are presented in Figures 4(d) and (e), respectively, with Port 1 radiating and all other ports terminated with 50 Ω impedance. At both resonant frequencies, surface currents are

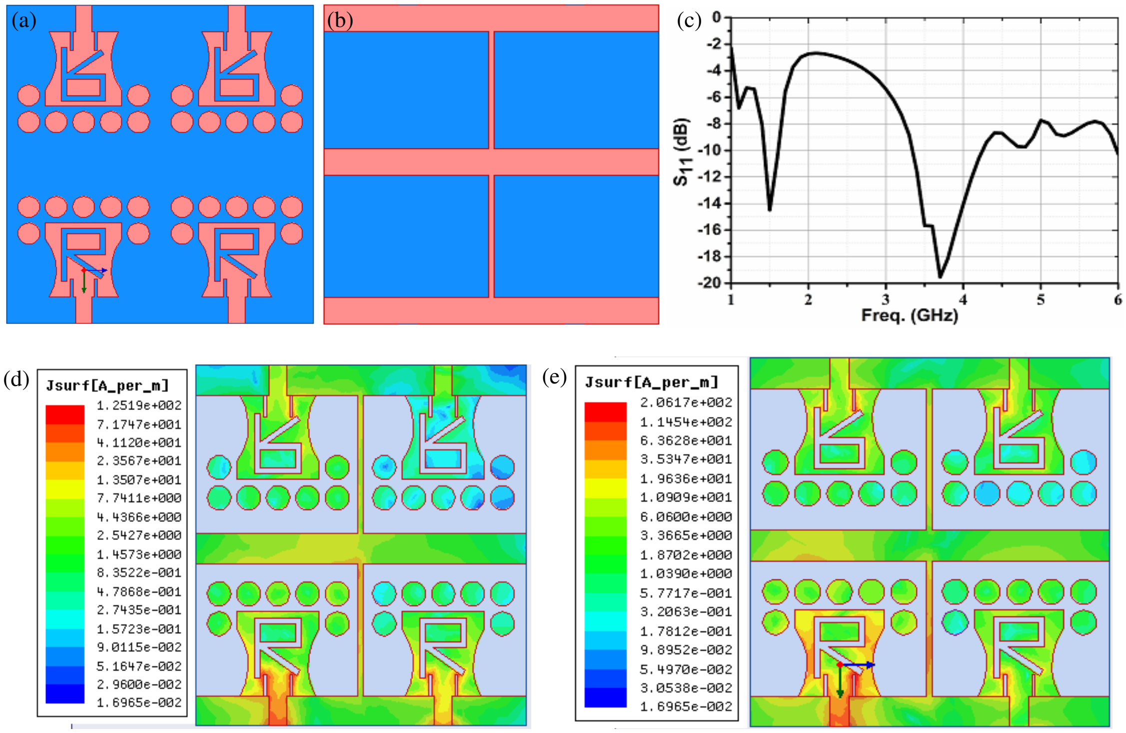

FIGURE 4. Four-element MIMO antenna. (a) Radiating element geometry (top view), (b) ground structure (bottom view), (c) S_{11} plot, (d) surface current distribution at 1.5 GHz, and (e) surface current distribution at 3.7 GHz.

mainly distributed along the feed line and the R-shaped antenna, proving their major role in antenna excitation. The current flows along the R-shaped slot, increasing the effective electrical path and thus providing the antenna resonance at two frequencies. In particular, more local concentration of the surface current in the inclined part of the R-shape proves responsible for higher resonant frequency and better impedance matching. It can be seen that no significant induced currents appear in the adjacent element, justifying the electromagnetic coupling suppression by the grid-like modification of the ground plane.

2.4. Implementation of the Proposed Eight-Element MIMO Antenna

The proposed eight-element MIMO antenna is represented by a set of eight identical radiating elements placed on a plane in a compact 4×2 arrangement with a grid-like ground plane configuration, as shown in Figure 5. As seen in Figure 5(a), the radiating elements are symmetrically arranged in two rows, where elements in the second row are flipped in the direction of orientation compared to the first row. This arrangement is vital for mutual coupling reduction, and one can observe that a proper distance exists between adjacent elements, along with parasitic elements in a circular configuration, which are intended to mitigate the effect of mutual coupling [10, 26]. Each of the radiating elements is placed next to a number of circular parasitic patches. Parasitic patches perform a passive decoupling role by disturbing the continuity of surface currents in neighboring elements. These are typically used to suppress surface waves and reduce mutual coupling between the closely spaced antenna elements. The antenna is fed using individual microstrip feed lines terminated with SMA connectors to excite each antenna separately. The vertical and horizontal spacing between adjacent antenna elements is described using the free-space wavelength at the lower operating frequency (1.8 GHz). Since $\lambda_0 = 166.7$ mm at 1.8 GHz, the vertical spacing of 12 mm is equal to $0.07\lambda_0$, and the horizontal spacing of 14 mm is $0.08\lambda_0$. This small spacing makes it possible to incorporate eight antenna elements in a small substrate area without poor isolation due to the designed decoupling technique.

As shown in Figure 5(b), the reverse side of the antenna has a grid-like modified ground plane, made from a set of metal strips, which reduces surface waves and improves impedance matching. The grid-like structure with specific spacing is designed to improve isolation, reducing mutual coupling between the eight elements, which is critical for MIMO performance. The "R-shape" allows the radiators to be electrically long while remaining physically small, helping fit eight distinct elements into a single compact printed circuit board (PCB). The fabricated prototype is highly consistent with the simulated design. Figure 5(c) shows the top-view photograph of the physical antenna fabricated on a dielectric substrate (FR4) using a chemical etching process. It shows the eight R-shaped copper radiators. Eight SMA connectors are soldered to the feed points, allowing each element to be tested independently. Figure 5(d) shows the fabricated ground plane. The copper strips correspond to the design and provide the necessary reference for the electromagnetic fields.

The graph shown in Figure 5(e) displays the simulated S_{11}, which indicates how much power is reflected back to the source. A value below -10 dB is generally considered a good

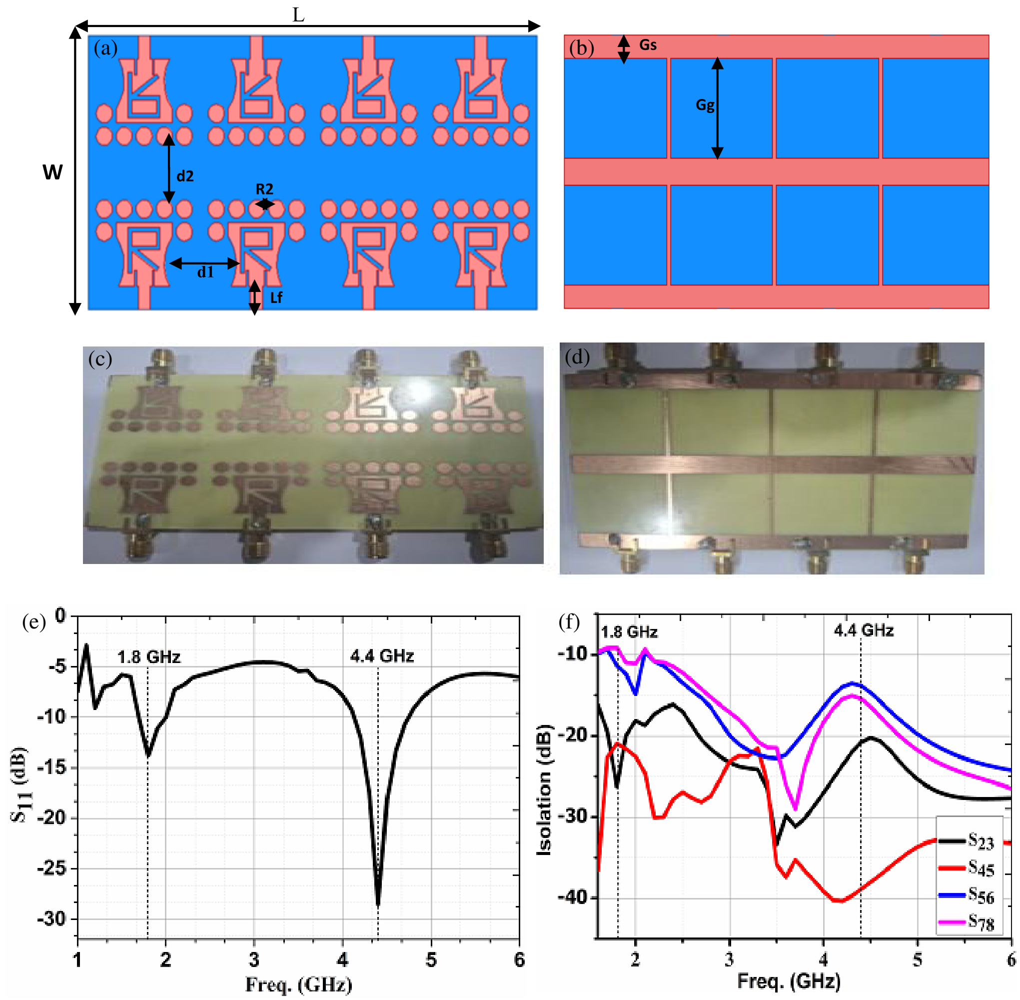

FIGURE 5. Proposed eight-element R-shaped MIMO antenna. (a) Top view of radiating element, (b) bottom view of ground plane, (c) photograph of the developed antenna (front), (d) rear view of the fabricated antenna, and (e) simulated S_{11}, and (f) isolation characteristics.

impedance match for operation. The eight-port MIMO antenna maintains dual-band performance. The S_{11} analysis demonstrates that the antenna exhibits good impedance-matching performance compared to the 4-element counterpart. Significant resonance occurs around the lower band (1.8 GHz), which is common for 4G LTE or GSM applications. A very sharp, deep resonance occurs at approximately 4.4 GHz (reaching −28 dB) in the higher band. The suggested eight-port radiator operates at dual bands with −10 dB impedance bandwidths of 360 MHz (1.67–2.03 GHz) and 600 MHz (4.15–4.75 GHz). The "dips" in the graph represent the frequencies, where the antenna efficiently radiates energy rather than reflects it. This improvement is due to the increased number of radiating elements, which introduces additional electromagnetic coupling paths and enhances current redistribution across the structure. The proposed MIMO antenna design uses a tight element separation distance 14 mm about 0.084λ at 1.8 GHz to achieve a very compact antenna design. Even with the tightly spaced elements, the proposed modified ground structure ensures that mutual coupling is kept to minimum. Figure 5(f) shows the simulated isolation performance of the proposed antenna between S_{23}, S_{45}, S_{56}, and S_{78} adjacent ports. As can be seen, mutual coupling between the neighboring antennas is more than 15 dB in the two operating bands (1.67–2.03 GHz and 4.15–4.75 GHz). As a result, the required isolation for the suggested compact MIMO structure is achieved. In terms of isolation, S_{45} exhibits the highest simulated isolation, approaching 40 dB near the upper operating band. Other adjacent ports achieve isolation levels between 15 dB to 30 dB. This enhancement in isolation performance can be attributed to the R-shaped radiator, circular parasitic elements, and grid-type modified ground, which can suppress surface waves and interaction between closely spaced antenna elements.

3. RESULTS AND DISCUSSION

The fabricated eight-port MIMO antenna was tested using a Vector Network Analyzer (VNA). The measurement setup using the VNA and placing the antenna in an anechoic chamber is shown in Figures 6(a)–(b). Both the simulated and measured results shown in Figure 6(c) indicate good matching capability with strong agreement between the outcomes. The minor discrepancies between the simulated and experimentally obtained results are inevitable due to possible deviations caused

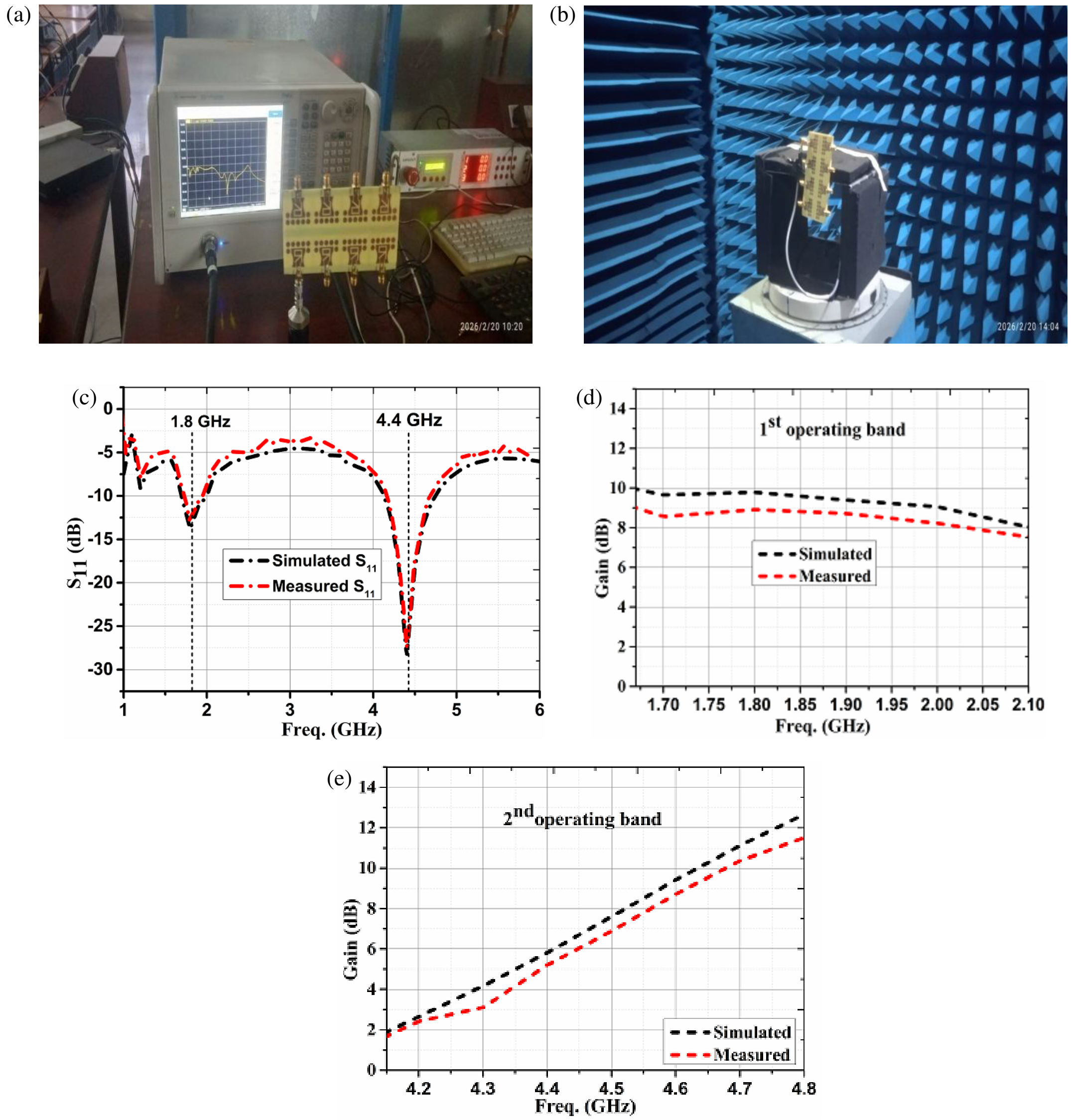

FIGURE 6. Experimental validation of the eight-element MIMO antenna: (a) Measurement setup using VNA, (b) radiation pattern measurement setup, (c) simulated versus experimental S_{11}, (d) frequency vs simulated & measured gain for 1st operating band, and (e) frequency vs simulated & measured gain for 2nd operating band.

by manufacturing inaccuracies, improper soldering, connector loss, and variations in the dielectric constant at high frequencies. The antenna's radiation pattern was measured by placing it on a rotating holder to acquire far-field radiation.

The simulated and experimental gains of the proposed antenna within the lower and higher frequency ranges are shown in Figures 6(d)–(e). The antenna's gain properties are consistent in both operational bands. As per simulation, in the lower band of operation (1.67–2.03 GHz), the gain is between 9 and 10 dB, and in the upper band (4.15–4.75 GHz), it gradually increases from 2 to 12 dB with linearity. The three-dimensional radiation patterns of the suggested R-shaped eight-element MIMO antenna are provided in Figure 7. In both 1.8 GHz and 4.4 GHz frequency ranges, the antenna shows consistent broadside radiation behavior in the direction of the positive z-axis. Some asymmetry and side-lobe levels have been seen in the patterns, which can be considered normal for any compact MIMO design with multiple elements due to the effects of coupling and geometrical discontinuity. However, there is no notable degradation of the main radiation lobe in operating bands.

The measured radiation patterns demonstrate consistent, reliable behavior at frequencies within the target band, which confirms the possibility of using the designed R-shaped antenna in practical applications. From the radiation pattern of the eight-port MIMO antenna design, it is evident that the antenna has a broadside radiation pattern, whereby the major gain occurs along the direction perpendicular to the substrate. The colour variation shows that there exists a gain gradient with the brighter regions indicative of high gains and the darker regions of low gains or radiation suppression. It is clear that the antenna has several secondary lobes, which can be attributed to array effects and inter-element couplings; however, there are no nulls or pattern distortion. This implies that the antenna has a sta-

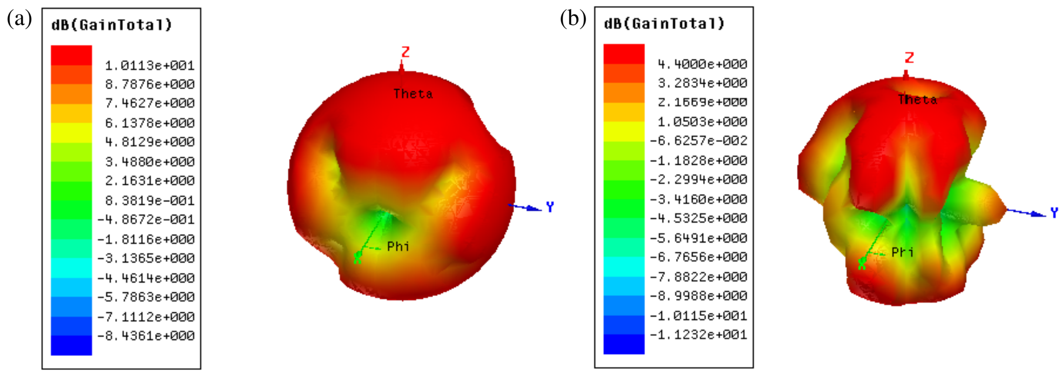

FIGURE 7. Simulated 3D radiation patterns for an eight-element MIMO antenna: (a) at 1.8 GHz and (b) at 4.4 GHz (The θ- and φ-coordinate axes are drawn to define their E-plane and H-plane positions, respectively.).

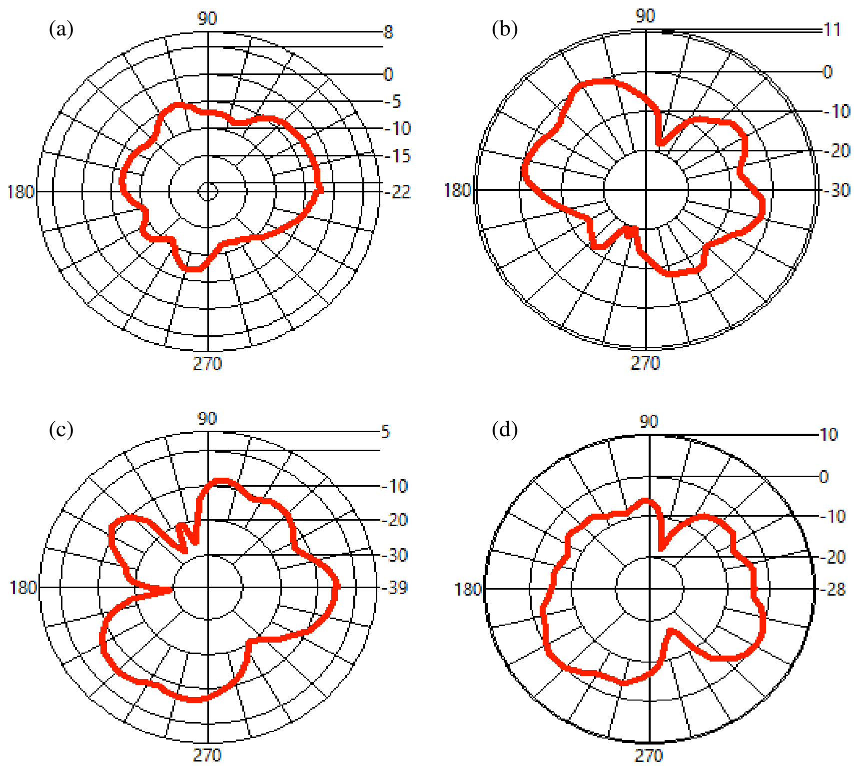

FIGURE 8. Radiation pattern measurements in 2-D planes. (a), (b) Radiation profile in the E-plane at 1.8 GHz. (c), (d) Radiation profile in the H-plane at 4.4 GHz.

ble radiation behavior and an even current distribution among the elements. Radiation characteristics of the proposed antenna are analyzed using polar plots in both E-plane and H-plane, as shown in Figures 8(a)–(d). At 1.8 GHz, the antenna exhibits a quasi-omnidirectional pattern with a relatively uniform power distribution, ensuring consistent coverage in the azimuth plane. The small distortions in the pattern can be attributed to mutual coupling and structural asymmetry. However, in the case of 4.4 GHz, the pattern takes a much more directional nature, marked by several side lobes with deeper nulls, due to higher-order mode excitation, along with a larger electrical size of the antenna. In the E plane, some lobe splitting is observed, and in the H plane, more fluctuation is noticed, indicating better directivity.

Figure 9 illustrates the simulated surface current distribution of the proposed grid-type MGS at two resonant frequencies of 1.8 GHz and 4.4 GHz. The proposed MGS is able to localize the surface current around the excited element and minimize current leakage to nearby radiators at both resonant frequencies. The high current concentration is confined only near the microstrip feed line and R-shaped radiator, whereas the modified ground plane impedes the surface-current path. Such localized current distribution proves that the proposed design retains the desired dual-band resonance and impedance matching while increasing the isolation of elements via suppressing mutual coupling. Furthermore, such a current distribution is consistent with the experimental results of S-parameters, which show that the isolation between adjacent ports stays above 15 dB across

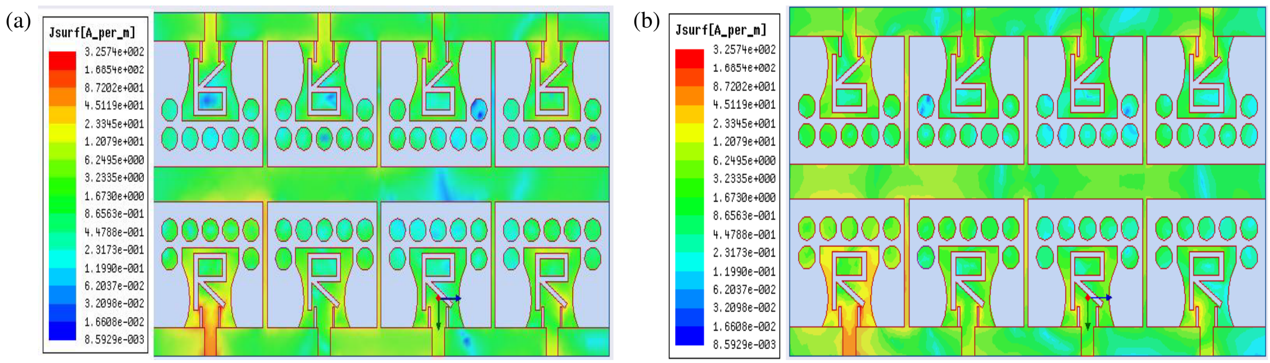

FIGURE 9. Simulated surface current distributions for the proposed MGS (a) at 1.8 GHz and (b) at 4.4 GHz.

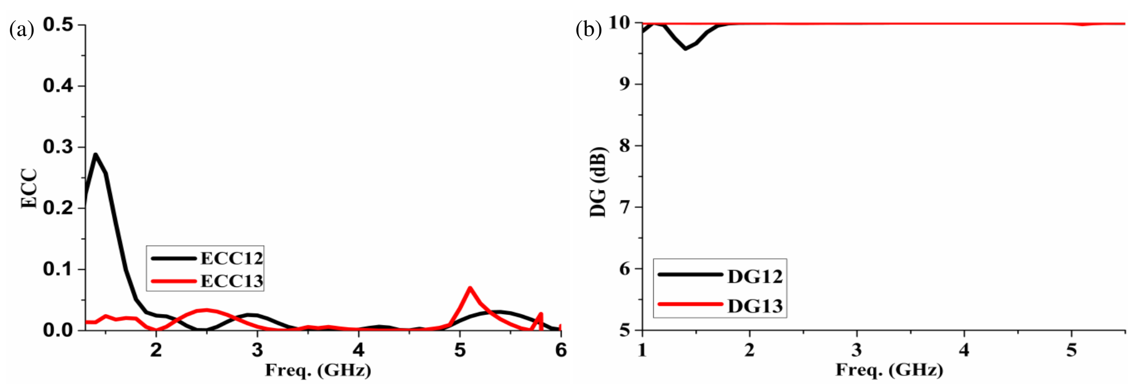

FIGURE 10. Diversity performance analysis of the MIMO antenna: (a) ECC between antennas Port 1–Port 2 and Port 1–Port 3, and (b) DG between antennas 1 and 2 & antennas 1 and 3.

TABLE 2. Comparative analysis of the developed eight-element MIMO antenna with reported antennas.

Ref.	Size (mm^2)	Frequency (GHz)	Isolation	ECC	Design Technique
[1]	150 × 75	3.4–3.65	> 15	< 0.01	E-slot and I-shaped frame
[2]	72 × 72	3.3–6.0	> 15	< 0.005	Fractal geometry
[11]	60 × 60	14–18	> 25	< 0.008	Neutralize block, parasitic elements, and DGS
[6]	150 × 75	3.2–6	> 12.6	< 0.31	MIMO array
[29]	150 × 80	3.4–3.6 4.6–4.8	> 17	< 0.05	Tunable MIMO
[15]	2400	at 3.5 GHz	> 20	< 0.00003	Metamaterial SRR
[30]	129 × 83	4.5–5.5	> 24	< 0.07	CPW based design with semi-arc stub
[26]	105 × 60	3.2–3.55	> 12	< 0.3	Coupled feed slots
Proposed	60 × 112	1.67–2.03 4.15–4.75	> 15 dB (Maximum ≈ 40 dB)	< 0.01	R-shape slot, circular parasitic elements, grid type modified ground plane

the operating bands and reaches 40 dB at certain resonant frequencies.

The antenna's diversity performance is evaluated using ECC and DG, which are key parameters for assessing reliability of a MIMO system. The computed ECC and DG values are shown in Figures 10(a)–(b). The ECC values are less than 0.01, and DG is approximately 10 dB, confirming excellent diversity performance. These results demonstrate that the proposed antenna is highly suitable for MIMO applications because it ensures reliable signal transmission with minimal interference between channels [12, 27]. ECC represents the level of inter-element correlation and signal reliability, respectively, and is vital for ensuring multi-path stability in sub-6 GHz wireless applications [16, 18]. It can be obtained using Equation (1) [27].

$$\mathrm{ECC}_{ij} = \frac{\left|\sum_{k=1}^{8} S_{ki} S_{kj}\right|^2}{\left(1-\left|\sum_{k=1}^{8} S_{ki}\right|^2\right)\left(1-\left|\sum_{k=1}^{8} S_{kj}\right|^2\right)} \tag{1}$$

where S_{ki}: scattering parameter from port k to port 1, S_{kj}: scattering parameter from port k to port j; i: antenna port indices; k: summation index over all ports. For an efficient MIMO antenna, the expected ECC is generally less than 0.5, whereas practical 5G systems require ECC < 0.1. For the proposed R-shaped MIMO antenna, ECC < 0.02, across 3.25–5.6 GHz. Diversity gain measures the improvement in signal reliability under multipath fading conditions. It is related to the ECC through Equation (2) [27].

$$\mathrm{DG} = 10\sqrt{1 - \mathrm{ECC}^2} \tag{2}$$

It is evident from Table 2 that the designed antenna shows promising performance compared with previously reported eight-element MIMO antennas. The antenna offers an in-band realized gain of about 9–10.5 dB in the lower operating band (1.67–2.03 GHz) and 2–12 dB in the upper operating band (4.15–4.75 GHz). Moreover, the designed antenna offers an isolation more than 15 dB in both operating bands; however, isolation up to 40 dB is obtained at particular resonant frequencies. Furthermore, the ECC is less than 0.01, reflecting good diversity [5, 28]. Although the proposed antenna has eight radiating elements, it maintains a small area of $60 \times 112\,\mathrm{mm}^2$. These features are attributed to the optimized R-shaped antenna and the use of the grid-shaped MGS, which efficiently controls the surface current.

4. CONCLUSION

The designed and simulated compact eight-element MIMO antenna, which uses innovative geometry-based design methodology to ensure high-efficiency operation in sub-6 GHz frequencies, proves the potential of a geometrical-driven approach to the development of highly efficient sub-6 GHz antennas. The novelty of this work can be seen in the dual-broadband nature of the used R-shaped antenna structure, which increases the length of the resonance circuit path without increasing physical length, as well as in using circular parasitic elements, which help improve impedance matching while decreasing mutual coupling between the elements, thus making EBGs or neutralization lines redundant. The 4×2 mirrored arrangement of antenna elements provides even more isolation. The antenna's S_{11} has a distinct value at 4.4 GHz, reaching -28 dB, implying very good impedance matching. The suggested antenna offers better than 15 dB isolation for adjacent ports in both working bands, with maximum isolation exceeding 30 dB and approaching up to 40 dB at certain resonant frequencies. The antenna shows stable broadside radiation pattern behavior with high directivity and stability in realized gain in both working bands, along with good MIMO diversity behavior, with ECC less than 0.01 and diversity gain of about 10 dB. The result shows that the designed antenna has high gain and isolation with a compact structure. The MIMO antenna proposed in this paper is well-suited for sub-6 GHz 5G systems. Nevertheless, in the coming years, more research will be done in order to enhance gain and bandwidth without changing its size. Using metasurfaces/metamaterials, reconfigurable components, and intelligent designs may improve the antenna's performance and therefore make it suitable for next-generation 5G and 6G systems.

REFERENCES

[1] Abubakar, H. S., Z. Zhao, B. Wang, S. H. Kiani, N. O. Parchin, and B. Hakim, "Eight-port modified E-slot MIMO antenna array with enhanced isolation for 5G mobile phone," *Electronics*, Vol. 12, No. 2, 316, 2023.

[2] Addepalli, T., M. S. Kumar, C. R. Jetti, N. K. Gollamudi, B. K. Kumar, and J. Kulkarni, "Fractal loaded, novel, and compact two- and eight-element high diversity MIMO antenna for 5G sub-6 GHz (N77/N78 and N79) and WLAN applications, verified with TCM analysis," *Electronics*, Vol. 12, No. 4, 952, 2023.

[3] Srivastava, G., V. Kumar, and A. Mohan, "Compact 8-port EMSIW MIMO antenna with high isolation for sub-6 GHz communication systems," *International Journal of Microwave and Wireless Technologies*, Vol. 16, No. 10, 1749–1755, 2024.

[4] Srivastava, G., V. Kumar, A. Kumar, A. Mohan, S. Kumar, and M. I. Hussein, "Low-profile compact integrated 16-port MIMO antenna covering sub-6 GHz and millimeter-wave 5G bands," *IEEE Access*, Vol. 13, 191 980–191 989, 2025.

[5] John, D. M., S. Vincent, S. Pathan, K. D. Shinde, B. S. Supreetha, and T. Ali, "Eight-element flexible MIMO antenna based on characteristics mode theory with enhanced channel capacity for sub 6 GHz 5G communications," *Results in Engineering*, Vol. 25, 104208, 2025.

[6] Jiang, J.-Y. and H.-L. Su, "A wideband eight-element MIMO antenna array in 5G NR N77/78/79 and WLAN-5 GHz bands for 5G smartphone applications," *International Journal of Antennas and Propagation*, Vol. 2022, No. 1, 8456936, 2022.

[7] Elabd, R. H., A. J. A. Al-Gburi, and A. A. Megahed, "Compact circular MIMO antenna with defected ground structure (DGS) for improved isolation in 5G sub-6 GHz mobile systems," *Results in Engineering*, Vol. 27, 105737, 2025.

[8] Kumar, P., S. Pathan, S. Vincent, O. P. Kumar, P. Kumar, P. R. Shetty, T. Ali, *et al.*, "A compact quad-port UWB MIMO antenna with improved isolation using a novel mesh-like decoupling structure and unique DGS," *IEEE Transactions on Circuits and Systems II: Express Briefs*, Vol. 70, No. 3, 949–953, 2023.

[9] Zhang, J., W. Luo, Q. Li, Y. Pan, and G. Liu, "Design and performance evaluation of a high-isolation MIMO antenna array for 5G N77/N78/N79 and WLAN implementations," *Progress In Electromagnetics Research B*, Vol. 110, 57–71, 2025.

[10] Kumar, B. P. and U. K. Kommuri, "High-gain eight-port dual-polarized magneto-electric dipole MIMO antenna array for 5G small-cell base station applications," *IEEE Access*, Vol. 14, 4013–4026, 2026.

[11] Khan, M. I., S. Liu, J. Mao, A. Basit, A. Ahmed, and A. Daraz, "Electromagnetic coupling suppression of eight-ports MIMO antenna for satellite communication with neutralize block and parasitic elements," *AEU — International Journal of Electronics and Communications*, Vol. 170, 154821, 2023.

[12] Tran, H.-H., T. T.-L. Nguyen, H.-N. Ta, and D.-P. Pham, "A metasurface-based MIMO antenna with compact, wideband, and high isolation characteristics for sub-6 GHz 5G applications," *IEEE Access*, Vol. 11, 67 737–67 744, 2023.

[13] Srivastava, G., A. Kumar, S. Rana, V. Kumar, A. Mohan, S. Kumar, and T. Ali, "Compact integrated self-multiplexing antenna for sub-6 GHz and millimeter wave 5G frequency spectrum," *Scientific Reports*, Vol. 16, 5457, 2026.

[14] Li, J., A. Jana, Y. Yuan, K. Zhang, S. N. Burokur, and P. Genevet, "Exploiting hidden singularity on the surface of the Poincaré

sphere," *Nature Communications*, Vol. 16, No. 1, 5953, 2025.

[15] Yuan, Y., K. Zhang, Q. Wu, S. N. Burokur, and P. Genevet, "Reaching the efficiency limit of arbitrary polarization transformation with non-orthogonal metasurfaces," *Nature Communications*, Vol. 15, No. 1, 6682, 2024.

[16] Al-Tameemi, A. R., G. C. Hock, T. S. Kiong, T. R. Al-Shaikhli, M. S. A. Ani, and M. A. K. Al Ani, "Analysis of isolation techniques for mutual coupling reduction in MIMO antennas," *Journal of Communications Software and Systems*, Vol. 21, No. 3, 348–359, 2025.

[17] Tamminaina, G. and R. Manikonda, "Design and analysis of wideband four-port multiple input multiple output antenna using defective ground structure for 5G communication," *International Journal of Electrical and Computer Engineering (IJECE)*, Vol. 14, No. 2, 1646–1653, 2024.

[18] Wang, Y., "Techniques for compact planar MIMO antennas," *MIMO Communications — Fundamental Theory, Propagation Channels, and Antenna Systems*, 2023.

[19] Salehi, M. and H. Oraizi, "Wideband high gain metasurface-based 4T4R MIMO antenna with highly isolated ports for sub-6 GHz 5G applications," *Scientific Reports*, Vol. 14, No. 1, 14448, 2024.

[20] Chen, Y.-T. and H.-L. Su, "A sub-6 GHz 8×8 MIMO antenna array for 5G metal-frame mobile phone applications," *Electronics*, Vol. 13, No. 23, 4590, 2024.

[21] Srinubabu, M. and N. V. Rajasekhar, "A compact and highly isolated integrated 8-port MIMO antenna for sub-6 GHz and mm-Wave 5G-NR applications," *Results in Engineering*, Vol. 25, 104068, 2025.

[22] John, D. M., T. Ali, S. Vincent, S. Pathan, J. Anguera, B. Virdee, R. M. David, K. Nayak, and S. P. Gopi, "A dual-band flexible MIMO array antenna for sub-6 GHz 5G communications," *Sensors*, Vol. 25, No. 11, 3557, 2025.

[23] Wong, K.-L., C.-Y. Wu, P.-C. Tsao, S.-W. Hsu, and W.-Y. Li, "Extremely low-profile four-antenna module covering U6 GHz band and its extreme receive antennas-aided MIMO application for 6G mobile devices," *IEEE Access*, Vol. 13, 156 785–156 798, 2025.

[24] Srivastava, G., A. Mohan, S. Kumar, H. C. Choi, and K. W. Kim, "Compact sixteen-port MIMO antenna for sub-6 GHz communications," *IEEE Access*, Vol. 13, 34 051–34 059, 2025.

[25] Mishra, B., R. Sethumadhavi, S. Singh, S. S. Sayeed, A. K. Singh, A. Pandey, and T. Ali, "An ultra-compact and high isolated 8×8 MIMO antenna system for 5G NR-n46 and n79 band applications," *Scientific Reports*, Vol. 16, No. 1, 12523, 2026.

[26] Morsy, M. M., "Compact eight-element MIMO antenna array for sub 6 GHz mobile applications," *SN Applied Sciences*, Vol. 5, No. 10, 261, 2023.

[27] Li, Y., W. Li, and W. Yu, "A multi-band/UWB MIMO/diversity antenna with an enhanced isolation using radial stub loaded resonator," *Applied Computational Electromagnetics Society Journal (ACES)*, Vol. 28, No. 1, 8–20, 2013.

[28] Raj, T., R. Mishra, A. Kapoor, D. Pandey, and S. Kundu, "A compact quad port MIMO antenna with gain augmentation using angularly stable and polarization insensitive FSS for 5G communication," *AEU — International Journal of Electronics and Communications*, Vol. 190, 155636, 2025.

[29] Sufyan, A., K. B. Khan, X. Zhang, T. A. Siddiqui, and A. Aziz, "Dual-band independently tunable 8-element MIMO antenna for 5G smartphones," *Heliyon*, Vol. 10, No. 4, e25712, 2024.

[30] John, D. M., S. Vincent, S. Pathan, A.-A. A. Boulogeorgos, J. Anguera, T. Ali, and R. M. David, "Eight element wideband antenna with improved isolation for 5G mid band applications," *Technologies*, Vol. 12, No. 10, 200, 2024.